PROCEEDINGS of the
24th International Congress on Acoustics
October 24 to 28, 2022 in Gyeongju, Korea

ABS-0313

Numerical simulation of the acoustic field around a violin

Masao YOKOYAMA[1]; Yuya ISHIGAKI[1]; Amane TAKEI[2]; Genki YAGAWA[3]

[1] Meisei University, Japan

[2] University of Miyazaki, Japan

[3] Toyo University and University of Tokyo, Japan

ABSTRACT

We numerically simulated the sound pressure field around the violin body using the finite-element method. Although there are many studies on the vibration and sound radiation of violins, obtaining results with a neat interpretation from a quantitative and qualitative standpoint remains a challenge. Herein, the highly precise geometry of the violin made by Stradivari was scanned with a micro-computed tomography scanner, where the material of the violin body was wood (spruce and maple) with orthotropic properties. This study aimed to clarify the relationship between the properties of wood and acoustic radiation around a violin vibrated by a force at the bridge.

Keywords: Sound, Insulation, Transmission

1. INTRODUCTION

We conducted numerical simulations of the vibration and sound radiation of violins made by old masters, such as the Antonio Stradivari and Guarneri families. Analyses using numerical simulations have been actively promoted since the beginning of the 21st century.[1] Computed tomography (CT) scanners have also been used to observe the internal structure of violins [2,3] and to investigate the material properties of wood.[4,5] Furthermore, methods using numerical simulation and/or CT scanners have been investigated as non-invasive and non-destructive methods for the analysis of historical assets such as violins.[6]

Previously, we conducted a coupled numerical simulation of violins using the finite-element method (FEM) and modeled the effects of wood properties on the vibration mode of the violin body.[7] This paper reports the measurement of the geometric data of a violin made by Stradivari using a micro-CT scanner, the relationship between the mode vibration and properties of wood, and the results of numerical simulations coupling the vibrations by a forced oscillation on a bridge with the acoustic field pressure around the violin.

2. GEOMETRIC DATA AND NUMERICAL SIMULATION

2.1 Three-dimensional geometry using a micro-CT scanner

The geometry of the violin made by Antonio Stradivari (1719) was scanned from the tailpiece to the scroll of the neck using a micro-CT scanner with a precision of 0.1 mm, as illustrated on the left side of Figure 1. The image on the right side of Figure 1 is a snapshot visualizing the interior of the violin body using scanned

[1] masao.yokoyama@meisei-u.c.jp

geometric data with computer-assisted design (CAD) software. As the scanned raw-geometric data include many fragments and holes, we must clean the data using CAD software before numerical simulation and visualization.

The import of geometric data, meshing, and FEM calculations were conducted using COMSOL Multiphysics™. The geometric data were divided into various parts, such as top and back plates, ribs, sound posts, and bass bars, to set different physical properties for each of them (Figure 2), and then saved as STEP files (standard for the exchange of product model data). The STEP files were imported into COMSOL Multiphysics as geometric objects. In addition, we set the spherical area of air surrounding the violin (Figure 2, right side). Points A–D represent the positions where the sound pressure was calculated in Section 3.2. In COMSOL Multiphysics, the mesh generator discretizes the domains into tetrahedral second-order mesh elements using the free-mesh method.[8] In total, there are approximately two million elements, including violins and air. The eigenmode frequency, displacement of the body, and sound pressure were calculated using the FEM via the acoustic-structure interaction module of COMSOL Multiphysics.

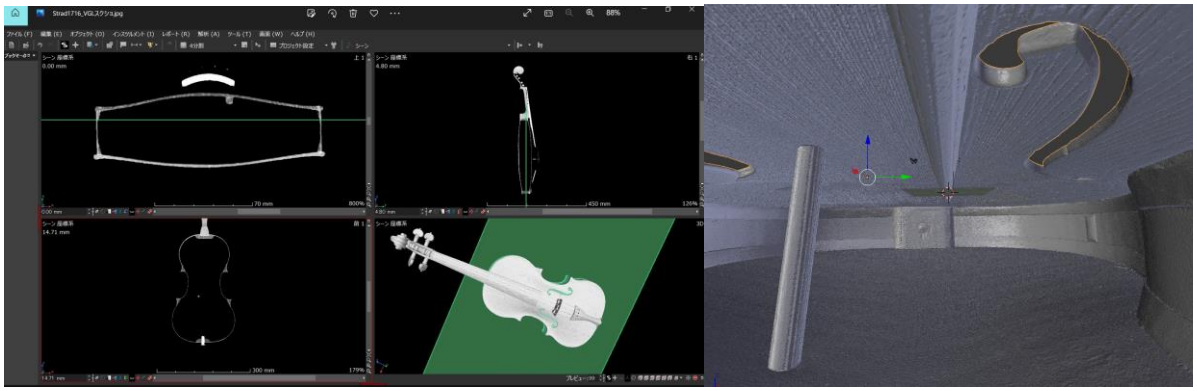

Figure 1 – View using the micro-computed tomography scanner and visualization of the interior of the violin using computer-aided design software

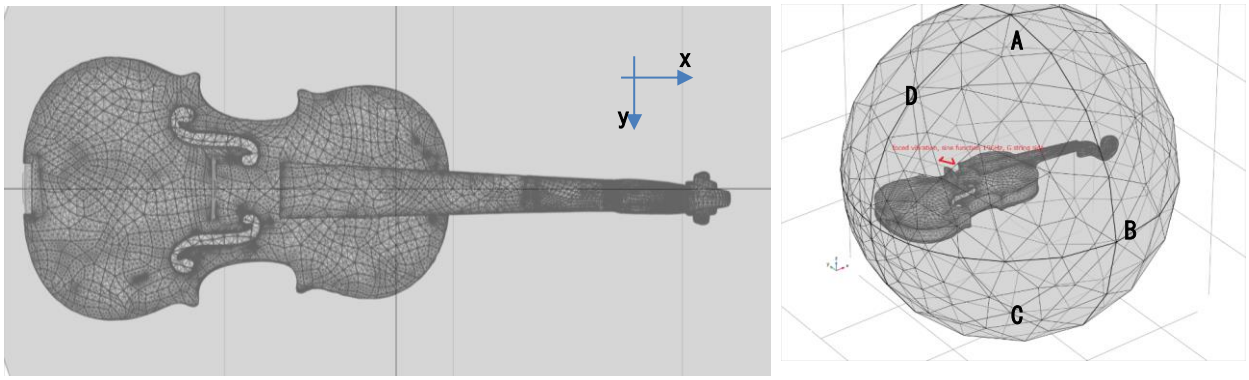

Figure 2 – Meshes of numerical simulation using the auto-mesh function of COMSOL Multiphysics. Points A–D is the position where the sound pressure is calculated in Section 3.2.

2.2 Parameter setting of the numerical simulation

The physical characteristics of wood can be set in three orthogonal directions in COMSOL Multiphysics: the longitudinal-grain direction (x-axis), radial annual-ring direction (y-axis), and direction tangential to the annual ring (z-axis). The typical values of the physical properties, such as Young's modulus, rigidity modulus, and Poisson's ratio, have been measured by Green et al.[9] The representative values of the density for maple and spruce are 0.63 and 0.36, respectively, and Young's moduli, Ex, are 12.6 GPa and 9.9 GPa, respectively. E_Y/E_X, E_Z/E_X, and the rigidity modulus (G/E_X) are the ratios of the longitudinal Young's modulus (EX) (Table 1).

Table 1 Values of orthotropic properties employed in the numerical simulation[9].
Ex value of maple is 12.6 GPa and that of spruce is 9.9 GPa.

Property	Maple	Spruce
Young's modulus E_Y / E_X	0.132	0.078
E_Z / E_X	0.065	0.043
Rigidity modulus G_{XY} / E_X	0.111	0.064
G_{YZ} / E_X	0.021	0.003
G_{XZ} / E_X	0.063	0.061
Poisson's ratio μ_{XY}	0.424	0.372
μ_{YZ}	0.774	0.435
μ_{XZ}	0.476	0.467

However, these values differed from the actual scanned values of the violins. We cannot disassemble and measure the properties of a cultural asset such as the Stradivari violin. Thus, we estimated the values for the numerical simulation using the frequency response function (FRF) of the scanned violin, as described in the next section.

3. SIMULATION RESULTS

3.1 Mode vibration and estimation of values of orthotropic properties

In this study, we estimated the orthotropic properties of wood to be set in the numerical simulation by comparing important eigenmode frequencies obtained by numerical simulation with those measured from the real Stradivari violin (1719) by FRF. In other words, this is an inverse problem where we estimate the values of the real properties of the wood by changing parameters such as density and Young's modulus in the numerical simulation and matching the eigenmode frequencies of the numerical simulation with those of the FRF.

The eigenmodes at low frequencies under 1,000 Hz, called A0, B1−, and B1+, were investigated in the vibration analysis of violins [1,2]. Figure 3 shows the FRF of the violin proposed by Stradivari (1719). Using a miniature hammer, we tapped the sides of the bridge on both the E and G strings and measured the results using an FFT analyzer. The peak on the left side of the graph (265 Hz) corresponds to the first air cavity mode, called A0. The next peaks were B1− (428 Hz) and B1+ (511 Hz), which were purported to influence the timbre of the sound.

Figure 4 shows the numerical simulation of the changes in the eigenfrequency owing to the changes in density

and E_X. The middle value in each graph represents the frequency calculated using the representative values.[9] This graph depicts eigenfrequencies with varying densities and E_X ranging from −20% to +20%. The free vibrations of the violin body were calculated without any constraint points.

Figure 4 shows that the eigenfrequency increased as E_X increased and decreased as the density increased. As shown in Table 2, the eigenfrequencies obtained by the numerical simulation using representative values were lower than those obtained by the FRF of the scanned violin. For instance, if we decrease the density of both maple and spruce by 10% and increase Ex by 10% (also E_Y, E_Z, and G), the eigenfrequencies obtained by the numerical simulation approach those obtained by the FRF.

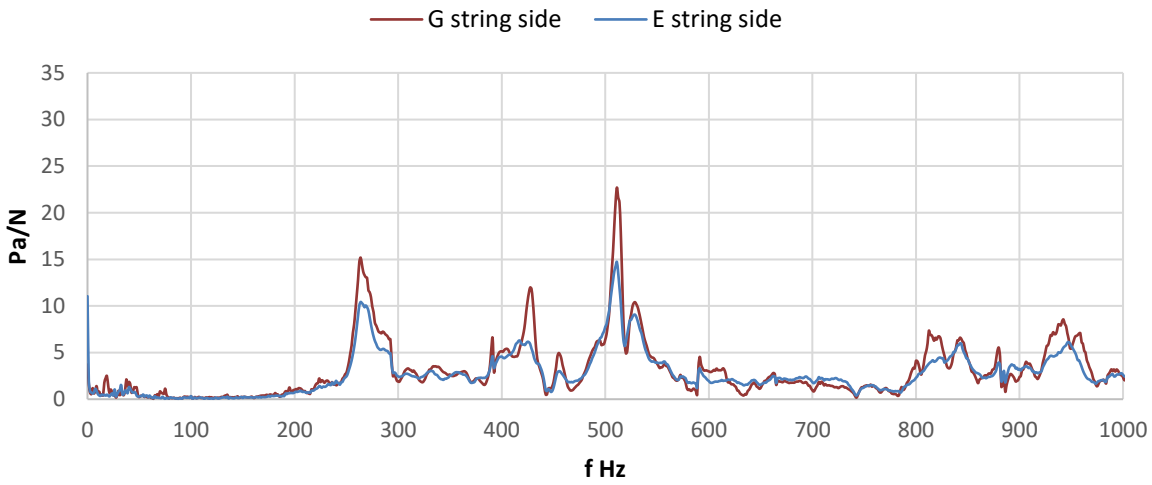

Figure 3 – Frequency response function of Stradivari (1719) from the hammering test.

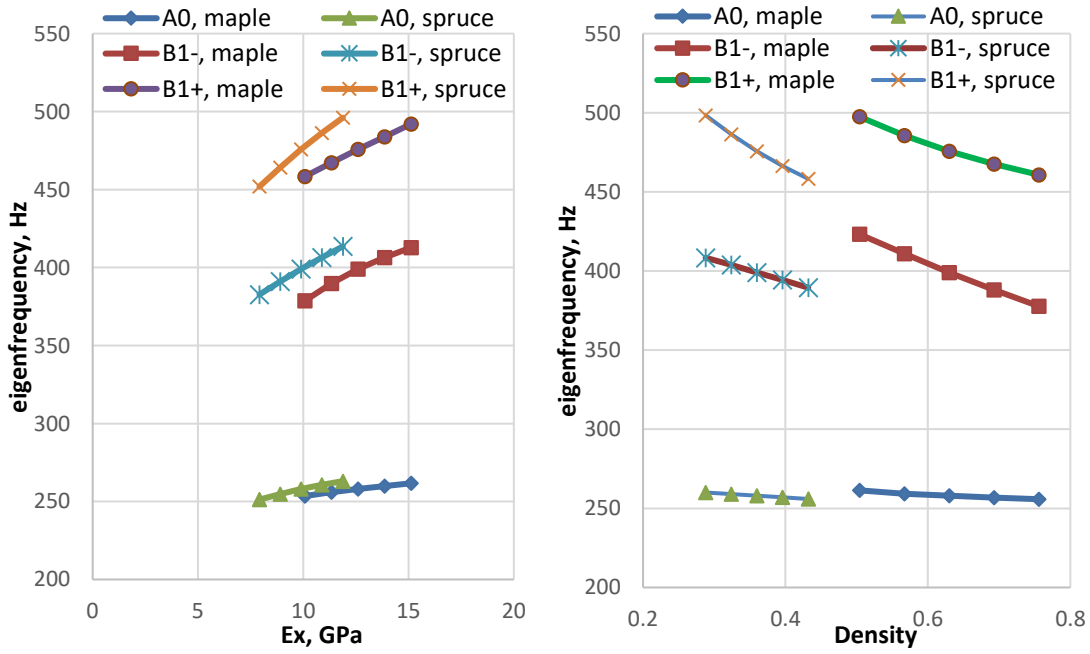

Figure 4 – Eigenfrequencies in the A0, B1−, and B1+ modes. The eigenfrequency increases with Young's modulus and decreases with the increasing density.

Table 2 – Comparison of the eigenfrequency (Hz): with the frequency response function (FRF) of Stradivari, numerical simulation with the representative value of the wood property[9], and with a decrease in density of 10% and increase in Ex of 10%.

	Experiment	Numerical simulation	
Mode	FRF (Strad. 1719)	Representative[9]	Density −10%, Ex +10%
A0	265	258	**265**
B1−	428	399	**431**
B1+	511	475	**516**

Figure 5 shows the displacement in the z-axis direction of the top/back plate in A0, B1 −, and B1+, which was calculated using the modified density and E_X, as mentioned above. The red area indicates where the displacement in the z-axis direction is positive, and the blue area indicates where it is negative.

In the A0 mode, the top plate bends widely on the bass bar side (left side of the violin in Figure 6 (a)). In the B1 mode, the top plate bends in the horizontal direction, and the back plate bends in the vertical direction. In contrast, the top plate bent in the vertical direction and the back plate bent in the horizontal direction in the B1+ mode. The displacement of the violin becomes asymmetrical because there is a sound post and bass bar inside the violin body. Other studies have found similar displacement patterns.[2]

Figure 6 shows the acoustic pressure fields around the violin in the numerical simulations. The radiation above the f-hole of the top plate was significant. The radiation under the back plate was also significant in the B1 mode. The sound radiation from the body appears to depend significantly on the bass bar and bend in the long-side direction (upper- and lower-bout directions).

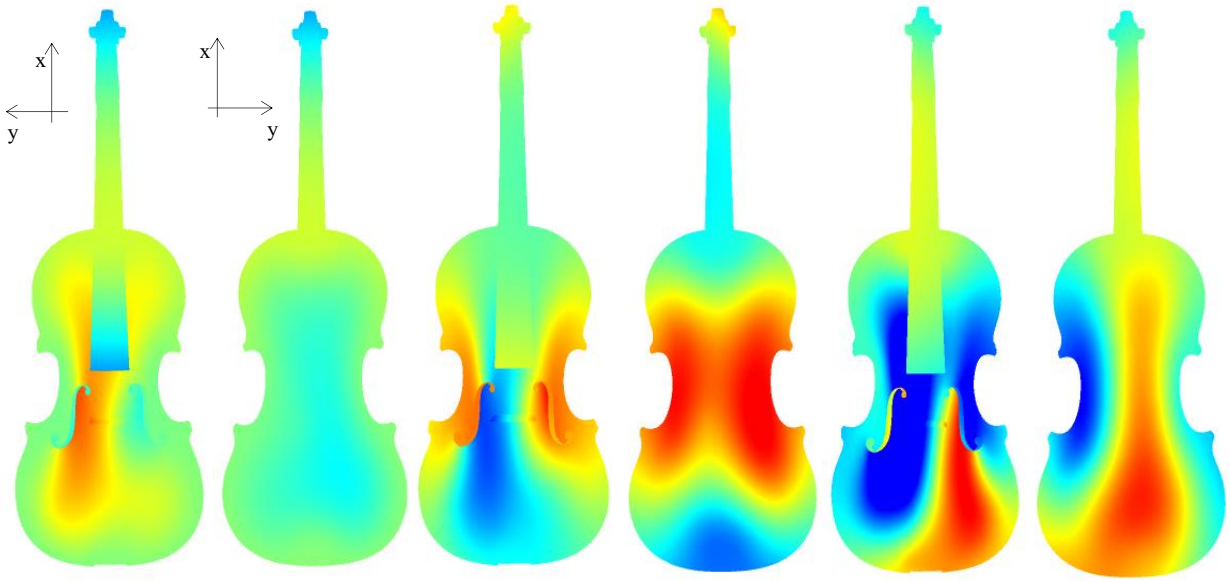

(a) mode A0, 265.0 Hz (b) mode B1−, 431.4 Hz (c) mode B1+, 516.1 Hz

Figure 5 – Displacement in A0, CBR, B1−, B1+ mode.

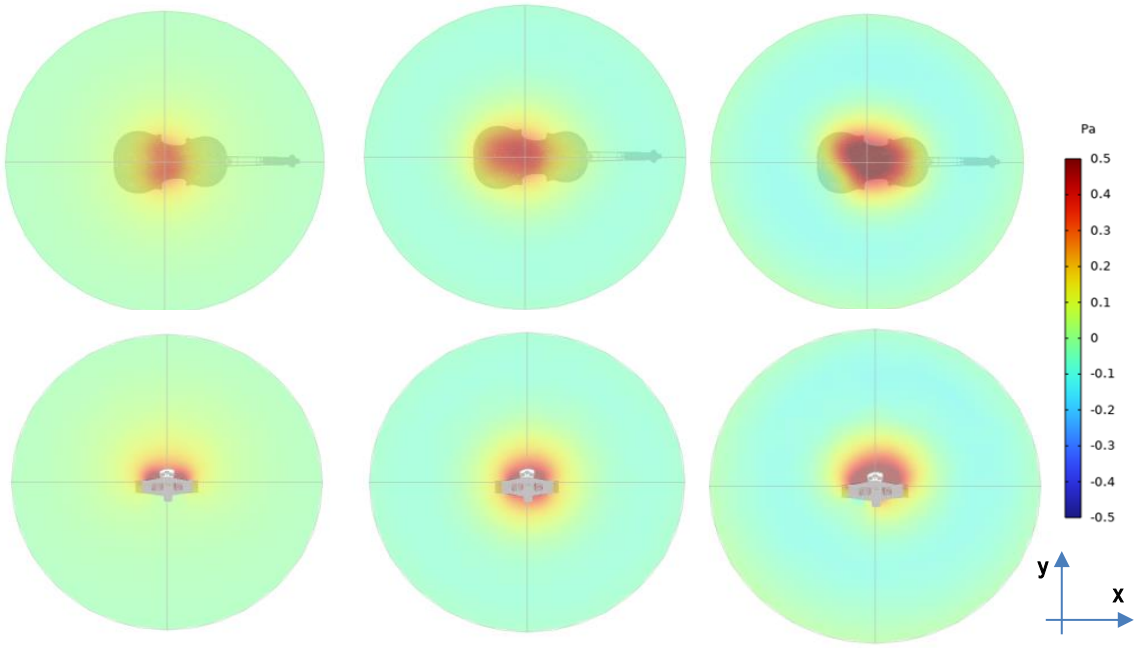

(a) mode A0, 265.0 Hz (b) mode B1−, 431.4 Hz (c) mode B1+, 516.1 Hz

Figure 6 – Sound radiation around the violin in the A0, B1−, and B1+ modes.

3.2 Acoustic pressure field around the violin in forced vibrations on the bridge

This section presents the simulation results when a forced sinusoidal oscillation is applied to the bridge of the violin. Figure 7 depicts the displacement of the body in the z-axis direction by forced vibrations. The right side of Figure 7 shows the oscillating position of the G string. The frequency of the sinusoidal function at 196 Hz (G3, the fundamental frequency of the G string) was inputted in the y-axis direction. On the left-hand side of Figure 7, the red area indicates where the displacement is positive and the blue area indicates where the displacement is negative.

The bridge alternately oscillated from side to side in the y-axis direction, and alternate vibrations of the top plate were induced by the bridge oscillation. In particular, the magnitude of the displacement on the bass bar side (the left side of the violin in Figure 7) was significant. We also speculated that the vibrations of the scroll and fingerboard do not significantly influence the sound volume and timbre; however, these vibrations are not negligible (see the video of detailed simulation results, https://youtu.be/m3cgG-TJs9Q).

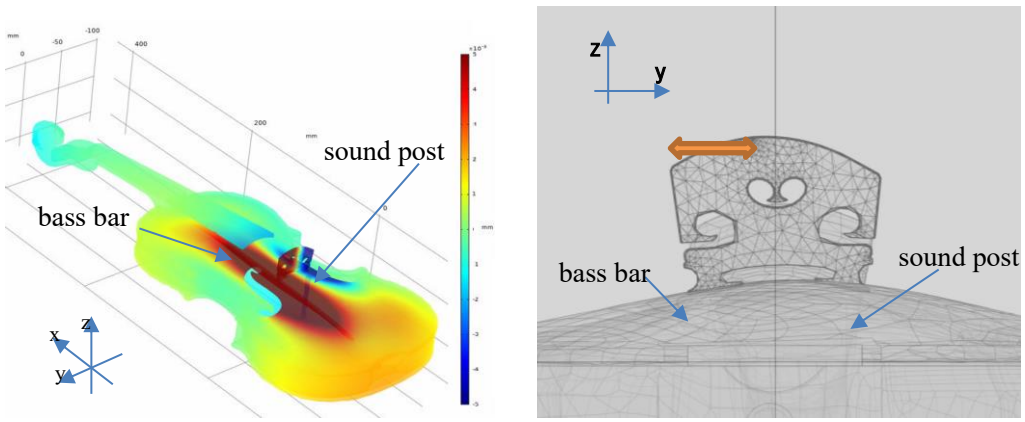

Figure 7 – Displacement of the violin by the forced vibrations on the bridge where the G string is placed (196 Hz). The bass bar side has significant vibrations. The scroll and fingerboard also vibrate.

The acoustic pressure fields in the y–z plane (including the bridge and sound post) and in the x–y plane (30 mm above the arch of the top plate) are shown in Figures 8 and 9, respectively. We simulated the vibration of the top plate by the sinusoidal oscillation of the bridge and concentric sound radiation from the f-hole and C-bouts. Similar to the experimental results obtained by Wang,[10] sounds at a low pitch radiated concentrically from the violin body. By contrast, the directivity of the sound was observed at a higher pitch. In the near future, we will numerically analyze the characteristics of sound radiation by varying the frequency and position of forced vibrations.

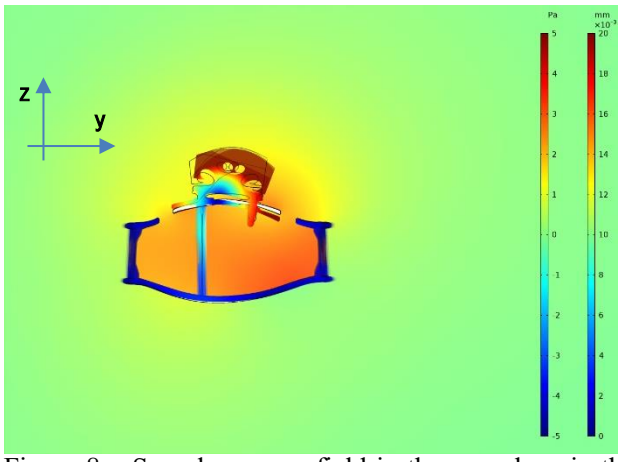

Figure 8 – Sound pressure field in the y–z plane in the forced vibrations with a sine wave of 196 Hz at the G

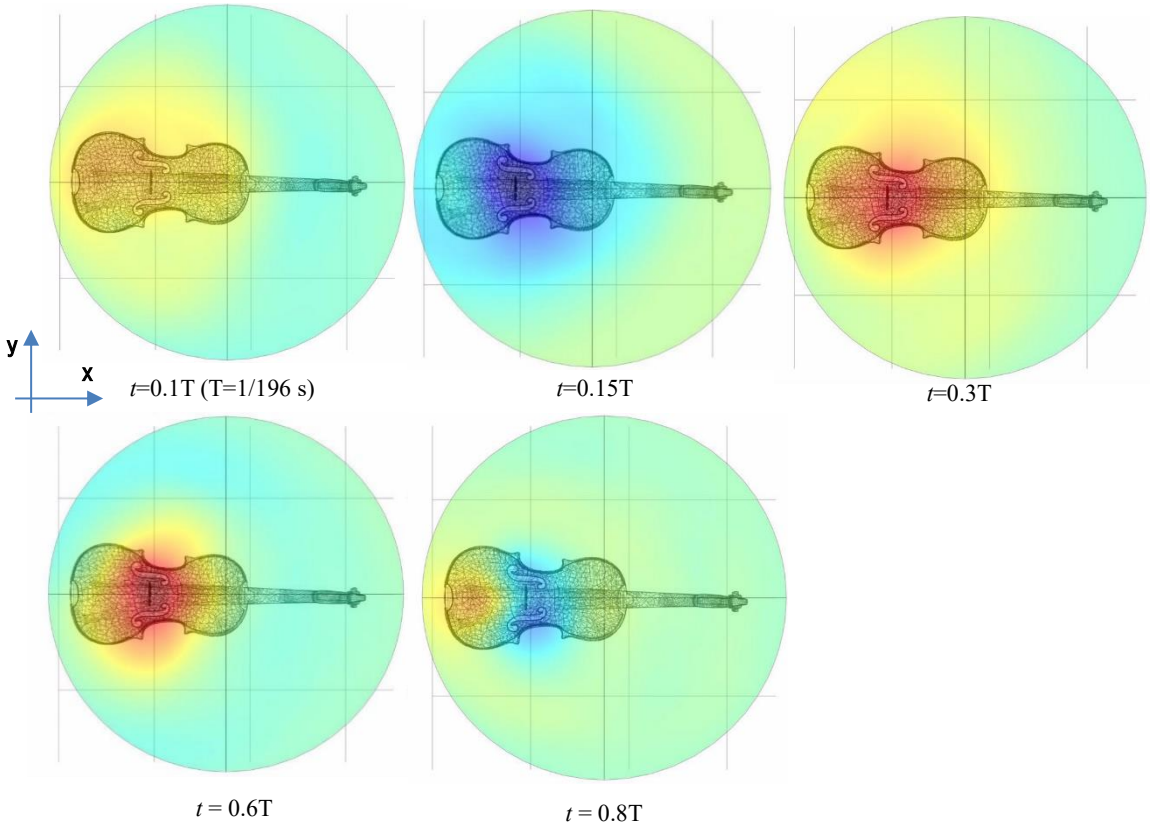

Figure 9 – Sound pressure fields around the body of the violin in the x–y plane 30 mm above the top of the arch.

Figure 10 shows the temporal change in acoustic pressure around the violin. Each line depicts the transition of the acoustic pressure at points A–D, as shown in Figure 2, during approximately two cycles of the sinusoidal function from the start of the forced oscillation (t = 0–0.01 s). The dotted line in the graph indicates the sinusoidal function of forced vibration on the bridge. The acoustic pressure at each point was similarly varied. Thus, we can also infer from the graph that the sound radiates concentrically when the bridge vibrates at 196 Hz with an open G string.

For instance, we can numerically simulate the directivity of sound radiation for the pitch difference. This

analysis of the acoustic field around the violin can be conducted experimentally in an anechoic chamber using array microphones. However, there are only a limited number of laboratories and facilities with anechoic chambers, and the cost is high. Thus, if we can substitute the numerical simulation for the experiment on sound radiation, coupled simulation can become an extremely useful tool.

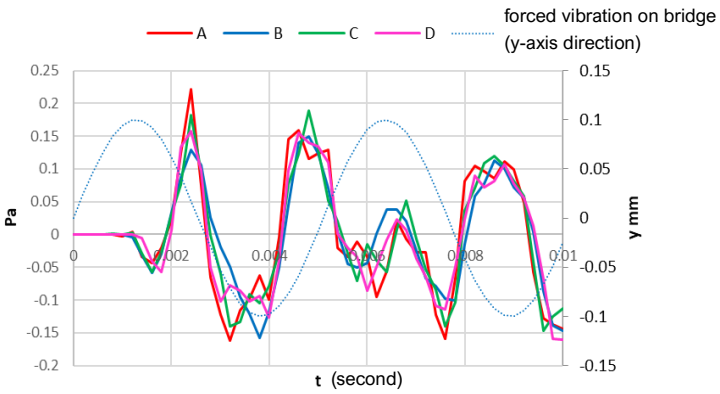

Figure 10 – Temporal change of sound pressure around the violin body at points A–D (in Figure 2).

4. CONCLUSIONS

A coupled simulation of the mode vibrations and sound radiation of a violin scanned by a micro-CT scanner was conducted using the FEM. We analyzed the relationship between the properties of wood and the eigenfrequency and visualized the vibration of the violin body and sound radiation in mode vibrations. Furthermore, we demonstrated that coupled simulation can analyze sound radiation. In future work, we intend to conduct a numerical simulation of sound radiation caused by string oscillations and analysis of sound radiation in a concert hall using a large-scale parallel computer.

ACKNOWLEDGEMENTS

The authors would like to thank Bunkyo-Gakki Co. Ltd. for providing violins. This study was supported by JSPS KAKENHI (grant number 21K11969).

REFERENCES

1. Gough, C. (2021). Acoustic characterization of string instruments by internal cavity measurements. The Journal of the Acoustical Society of America, 150(3), 1922–1933.
2. Bissinger, G. and Oliver, D. (2007). 3-D laser vibrometry on legendary old Italian violins. Sound and Vibration, 41(7), 10–15.
3. Borman, T. and Stoel, B. (2009). Review of the uses of computed tomography for analyzing instruments of the violin family with a focus on the future. J Violin Soc Am: VSA Papers, 22(1), 1–12.
4. Stoel, B. C., Borman, T. M., and De Jongh, R. (2012). Wood densitometry in 17th and 18th century Dutch, German, Austrian and French violins, compared to classical Cremonese and modern violins. PLoS One, 7(10).
5. Stanciu, M. D., Mihălcică, M., Dinulică, F., Nauncef, A. M., Purdoiu, R., Lăcătuș, R. and Gliga, G. V. (2021). X-ray Imaging and computed tomography for the identification of geometry and construction elements in the structure of old violins. Materials, 14(20), 5926.
6. Sodini, N., Dreossi, D., Chen, R., Fioravanti, M., Giordano, A., Herrestal, P. and Zanini, F. (2012). Non-invasive microstructural analysis of bowed stringed instruments with synchrotron radiation X-ray microtomography. Journal of Cultural Heritage, 13(3), S44–S49.
7. Yokoyama, M. (2021). Coupled numerical simulations of the structure and acoustics of a violin body. The Journal of the Acoustical Society of America 150(3), 2058–2064.
8. Acoustic-Structure Interaction, COMSOL Homepate, https://www.comsol.jp/model/acoustic-structure-interaction-417.
9. Green, D. W., Winandy, J. E. and Kretschmann, D. E. (1999). Mechanical properties of wood. Wood handbook: Wood as an engineering material. Madison, WI: USDA Forest Service, Forest Products Laboratory. General technical report FPL; GTR-113: 4.1-4.45, 113.
10. Wang L. M. and Burroughs C. B., (2001). Acoustic radiation from bowed violins, Journal of the Acoustical Society of America. 110(1), 543–555.